



Contents lists available at ScienceDirect

Tectonophysics

journal homepage: www.elsevier.com/locate/tecto

Dispersion of elastic moduli in a porous-cracked rock: Theoretical predictions for squirt-flow

M. Adelinet ^{a,b,*}, J. Fortin ^a, Y. Guéguen ^a^a Laboratoire de géologie, École normale supérieure, UMR CNRS 8538, France^b LGRMP, Université du Maine, UMR CNRS 6112, France

ARTICLE INFO

Article history:

Received 18 March 2010

Received in revised form 23 July 2010

Accepted 12 October 2010

Available online xxx

Keywords:

Frequency dispersion

Rock properties

Bimodal porosity

Effective medium theory

Poroelectricity theory

Elastic waves velocities

ABSTRACT

Crustal rocks contain variable amount of both cracks and equant pores depending on tectonic and thermal stresses but also on their geological origin. Crack damage and porosity change result in effects on elastic waves velocities. When rocks are fluid saturated, dispersion of the P- and S-waves should be taken into account. This paper deals with frequency dispersion of elastic moduli in a fluid saturated porous and cracked rock with the assumption that squirt-flow is the dominant process. We develop a theoretical approach to calculate both high (HF) and low (LF) frequency bulk and shear moduli. The HF moduli are derived from a new effective medium model, called CPEM, with an isotropic distribution of pores or cracks with idealized geometry, respectively spheres and ellipsoids. LF moduli are obtained by taking HF dry moduli from the CPEM and substituting into Gassmann's equations. In the case of a porosity only supported by equant pores, the calculated dispersion in elastic moduli is equal to zero. In the case of a crack porosity, no bulk dispersion is predicted but a shear dispersion appears. Finally in the general case of a mixed porosity (pores and cracks), dispersion in bulk and in shear is predicted. Our results show that the maximum dispersion is predicted for a mixture of pores and spheroidal cracks with a very small aspect ratio ($\leq 10^{-3}$). Our theoretical predictions are compared to experimental data obtained during hydrostatic experiment performed on a basaltic rock and a good agreement is observed. We also used our theoretical model to predict elastic waves velocities and Vp/Vs ratio dispersion. We show that the P-waves dispersion can reach almost 20% and the Vp/Vs dispersion a maximum value of 9% for a crack porosity of about 1%. Since laboratory data are ultrasonic measurements and field data are obtained at much lower frequencies, these results are useful for geophysicists to interpret seismic data in terms of fluid and rock interactions.

© 2010 Elsevier B.V. All rights reserved.

1. Introduction

An important area of geophysical research is based on elastic property variations in rocks due to fluid content/microstructure coupling. This effect is extremely dependent on the strain frequencies at which rocks are submitted (Guéguen et al., 2009). At seismic frequencies (typically less than 1 kHz), fluid pressure has time to reach equilibrium in rocks and poroelastic theory is correct to describe elastic properties (Gassmann, 1951; Biot, 1956; Murphy, 1985). At laboratory frequencies (typically more than 10 kHz), the poroelastic assumption of fluid pressure equilibrium inside the pore space becomes invalid. At such high frequencies, stress can induce fluid flow from one inclusion to another (Mavko and Nur, 1975; Dvorkin and Nur, 1993; Dvorkin et al., 1995). Such a process of squirt-flow is described on Fig. 1 between two cracks and between one crack and one equant pore. The crack orientation, relative to the compressive

stress, controls the fluid pressure gradients. As a consequence, the Biot-Gassmann equations underestimate the rock elastic properties in the high frequency range. This process is the only one considered in this paper.

To predict HF moduli, a theoretical model based on rock microstructure is necessary. However natural rock can be extremely heterogeneous. To obviate this problem an assumption is necessary. We consider a representative element volume (REV) in a medium that is statistically homogeneous. It means that any part of the system with a volume larger than the REV has identical properties. From literature, a lot of inclusion-based models exist to express elastic moduli in HF range. They usually relied on effect of inclusions on stress/strain elastic field disruption following Eshelby (1957)'s theory. In order to improve the effective medium theory, various schemes have been derived. The simplest one is the dilute model (non-interaction approximation). The self-consistent scheme (SCS) and the differential approach (DEM) are two possible ways to account approximately for interactions. The SCS model is based on the following idea: a single inclusion is embedded within a large matrix whose properties are those of an effective matrix (Budiansky and O'Connell, 1976). In the

* Corresponding author. Now at IFP Energies nouvelles, 1-4 avenue de Bois-Préau, 92852 Rueil-Malmaison cedex, France. Tel.: +33 147527142; fax: +33147527098.

E-mail address: mathilde.adelinet@ifpenergiesnouvelles.fr (M. Adelinet).

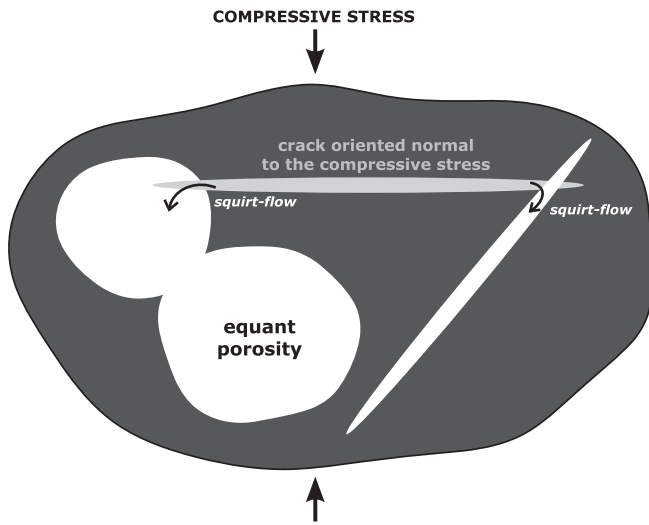


Fig. 1. Sketch of the squirt-flow process which occurs at high frequencies. The fluid flow takes place from over-pressured areas (grey crack) to under-pressured areas (white crack and equant pores).

DEM approach, several inclusions are introduced in a well-identified matrix one by one. An iterative treatment is applied to obtain elastic moduli step by step (Henyey and Pomphrey, 1982; Norris, 1985; Le Ravalec and Guéguen, 1996a,b). We used in the following, the non-interaction approximation (NIA). Inclusions are introduced simultaneously into the free-inclusion matrix whose properties are those of the bulk material (Kachanov, 1993; Schubnel and Guéguen, 2003;

Fortin and Guéguen, 2007). Using the NIA, the effective elastic properties can be completely calculated as functions of the crack geometry and pore distribution (Bristow, 1960; Walsh, 1965; Kachanov, 1980, 1993). One of the input data of all effective medium models is the geometry of the rock porosity. Depending on authors and models, the pore structure can be described as a continuous spectrum of pore shapes or as a segregation into two categories: equant pores and very thin cracks.

In this study, a new effective medium model is developed to calculate dry and saturated HF moduli for a porous-cracked medium. The LF saturated moduli are estimated by using the dry moduli and the Gassmann equations. Frequency dispersion is defined as the normalized difference between HF elastic moduli calculated from effective medium modeling and LF elastic moduli calculated from poroelastic theory. The sketch of the theoretical proposed method is summarized in Fig. 2.

Our theoretical predictions highlight the role played by cracks which are the major cause of elastic properties modifications. The theoretical method and its predictions are given in Sections 2 and 3. In addition, our theoretical predictions are compared with other modeling studies (Endres and Knight, 1997; Le Ravalec and Guéguen, 1996b) and compared to experimental data (HF and LF bulk moduli) obtained on an Icelandic basalt (Adelinet et al., 2010), which is a cracked-porous rock (Section 4). Finally the P- and S-waves velocities dispersion, i.e. the expected dispersion between seismic waves velocities measured in the field and ultrasonic waves velocities measured in the laboratory is predicted as well as Vp/Vs ratio dispersion. Note that for these predictions we chose to limit the calculations to a crack fraction range compatible with natural data, i.e. equivalent to a crack porosity smaller than 2%, which is the case of the most common crustal rocks (Section 5).

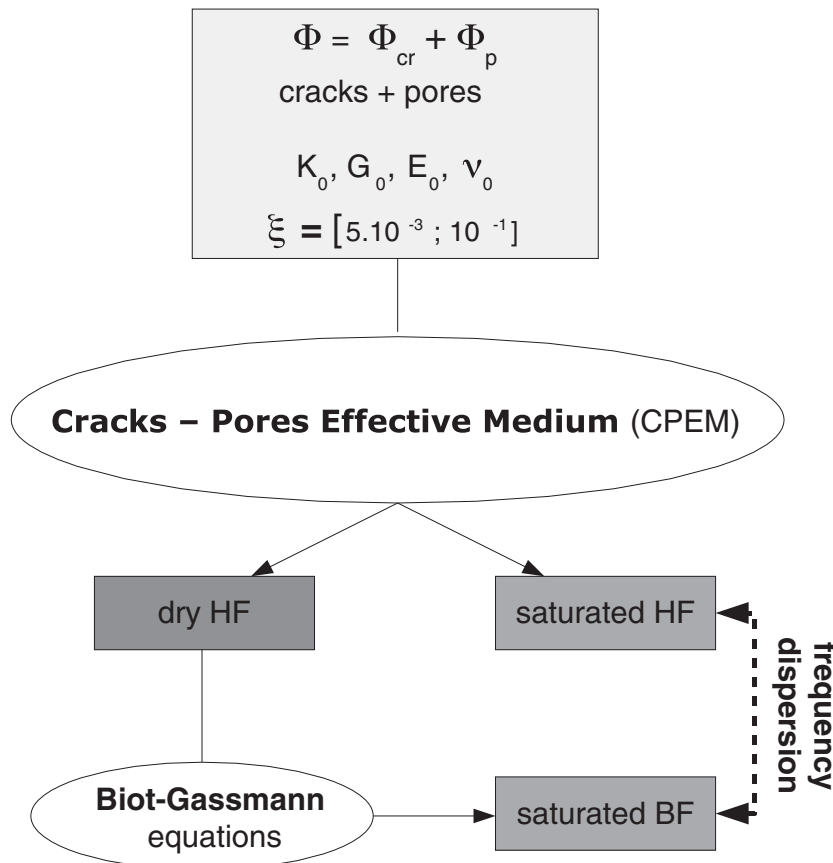


Fig. 2. Sketch of the method. Input data in CPEM are on the top, output data are HF and LF moduli, double arrows stay for dispersion calculation. Φ stays for the global porosity, Φ_p for the equant porosity, Φ_{cr} for the crack porosity and ξ for the crack aspect ratio.

2. Theoretical tools

2.1. HF moduli calculation

One of the objectives of this study is to build a model simple enough to obtain closed formulations for bulk and shear moduli but yet sophisticated to take into account the physical processes when frequency effect occurs.

Based on the works of [Kachanov \(1993\)](#); [Kachanov et al. \(1994\)](#); [Shafiro and Kachanov \(1997\)](#), a specific effective medium, called CPEM (Cracks and Pores Effective Medium) is presented in this study in order to calculate bulk and shear HF moduli, noted as K_{HF} and G_{HF} . In this model spheroidal cracks and equant pores are embedded in a well-identified matrix ([Fig. 3](#)). The cracks are randomly distributed in orientation within the matrix. The global porosity Φ of the CPEM can be written as the sum of two terms:

$$\Phi = \Phi_p + \Phi_{cr}, \tag{1}$$

where Φ_p is the equant porosity and Φ_{cr} the crack porosity.

Such a mixed model has already been used in [Fortin and Guéguen \(2007\)](#) but here different assumptions are made. Firstly we chose to use the Non-Interaction Assumption (NIA). The low investigated porosities (<10%) make this approximation valid in regards with conclusions of [Guéguen et al. \(1997\)](#). Note that there is no conflict between the NIA and the existence of connections that allow fluid flow between adjacent parts of the pore–crack network at suitably low frequencies. Second we use in this model spheroidal cracks instead of penny-shaped geometry used in [Fortin and Guéguen \(2007\)](#). Penny-shaped cracks are very useful to estimate transport properties in cracked rocks ([Guéguen and Dienes, 1989](#)) but less convenient to calculate HF saturated elastic moduli when fluid is present in the medium.

The goal of this section is to introduce the results required to express the HF elastic properties of a porous-cracked rock. The effective medium theory is used to calculate the additional terms corresponding to extra stiffness and extra compliance due to presence of pores and cracks. The two different cases are firstly studied independently before focusing on the mixed model.

2.1.1. A simple medium with only equant pores

Considering an effective medium with only equant pores, we introduce the parameter δ_p to characterize the coupling between matrix compliance, fluid compressibility and equant pore geometry ([Kachanov, 1993](#)):

$$\delta_p = \frac{2E_0}{9(1-\nu_0)} \left(\frac{1}{K_f} - \frac{1}{K_0} \right), \tag{2}$$

where E_0 , K_0 and ν_0 are the elastic parameters of the free-inclusion matrix, respectively the Young modulus, the bulk modulus and the Poisson ratio. K_f is the fluid bulk modulus. In the following sections we also use G_0 for the shear modulus of the free-inclusion matrix.

In the saturated case, the stress perturbation due to equant pores is taken into account and the bulk and shear effective moduli (respectively K_{HF}^{sat} and G_{HF}^{sat}) can be derived following [Zimmerman et al. \(1986\)](#); [Shafiro and Kachanov \(1997\)](#) as

$$\frac{K_0}{K_{HF}^{sat}} = 1 + \Phi_p \frac{3(1-\nu_0)}{2(1-2\nu_0)} \left(\frac{\delta_p}{1 + \delta_p} \right), \tag{3}$$

$$\frac{G_0}{G_{HF}^{sat}} = 1 + \Phi_p \frac{15(1-\nu_0)}{7-5\nu_0}. \tag{4}$$

The effective bulk and shear moduli can be deduced from Eqs. (3) and (4) for the dry case using $\delta_p \rightarrow \infty$ ([Kachanov, 1993](#)) so that $\frac{\delta_p}{1 + \delta_p} \rightarrow 1$. The shear effective modulus has the same expression in the dry and wet cases.

2.1.2. A simple medium with only spheroidal cracks

Let us consider a randomly oriented spheroidal crack population ; the crack porosity Φ_{cr} is related to the aspect ratio ξ and the crack density ρ using

$$\Phi_{cr} = \frac{4}{3} \pi \rho \xi. \tag{5}$$

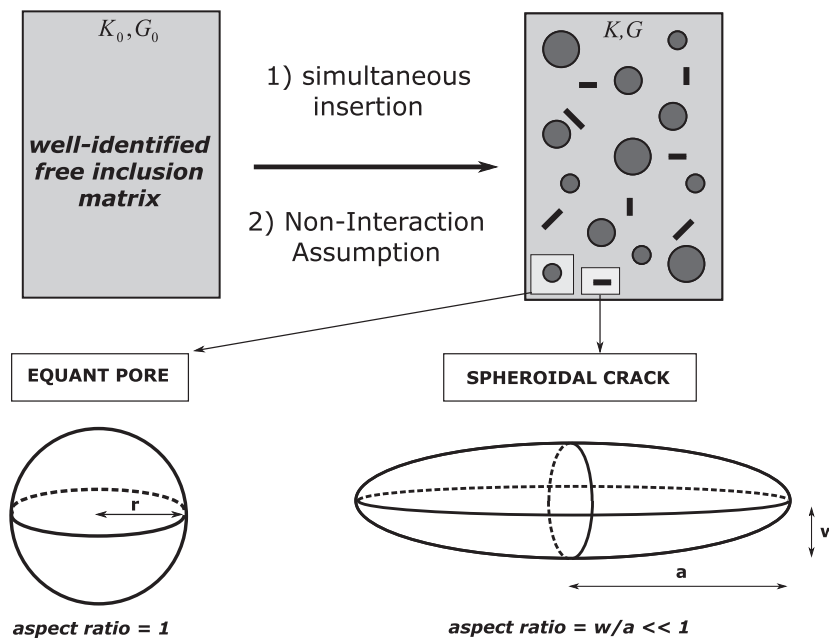


Fig. 3. Sketch of the present effective medium model: we consider a mixture of spheroidal cracks and equant pores. We also used the Non-Interaction Assumption (NIA).

Aspect ratio and crack density are respectively defined as $\xi = \frac{\omega}{c}$ and $\rho = \frac{1}{V} \sum_i^n c_i^2$ where ω and c are the lengths of the spheroid semi-axis (see Fig. 3), V the Representative Elementary Volume and n the number of cracks.

Porosity and crack parameters (ξ and ρ) are the key parameters which control the different physical properties. Like for the effective medium with only equant pores, a parameter δ_c is used to characterize the coupling between matrix compliance, fluid compressibility and crack geometry:

$$\delta_c = \frac{E_0 \pi \xi}{4(1-\nu_0^2)} \left(\frac{1}{K_f} - \frac{1}{K_0} \right). \quad (6)$$

In the saturated case, the normal compliance of a crack is changed due to fluid saturation and the parameter δ_c should be taken into account for the bulk and shear moduli. Bulk and shear moduli can be derived following (Kachanov, 1993) as

$$\frac{K_0}{K_{HF}^{sat}} = 1 + \rho \frac{16(1-\nu_0^2)}{9(1-2\nu_0)} \left(\frac{\delta_c}{1 + \delta_c} \right), \quad (7)$$

$$\frac{G_0}{G_{HF}^{sat}} = 1 + \rho \left[\frac{16(1-\nu_0)}{15(1-\frac{\nu_0}{2})} + \frac{32(1-\nu_0)}{45} \left(\frac{\delta_c}{1 + \delta_c} \right) \right]. \quad (8)$$

As mentioned above, the dry moduli can be deduced from Eqs. (7) and (8) using $\delta_c \rightarrow \infty$ ($\frac{\delta_c}{1 + \delta_c} \rightarrow 1$).

2.1.3. CPEM used equations

We consider in this section the CPEM model based on the mixture of spheroidal cracks and equant pores. Using an assumption of non-interaction between cracks and pores, we can calculate the HF bulk and shear moduli for the saturated isolated regime in which there is no fluid flow between inclusions using a combination of Eqs. (3)–(7) and Eqs. (4)–(8). This leads to:

$$\frac{K_0}{K_{HF}^{sat}} = 1 + \Phi_p \frac{3(1-\nu_0)}{2(1-2\nu_0)} \left(\frac{\delta_p}{1 + \delta_p} \right) + \rho \frac{16(1-\nu_0^2)}{9(1-2\nu_0)} \left(\frac{\delta_c}{1 + \delta_c} \right), \quad (9)$$

$$\frac{G_0}{G_{HF}^{sat}} = 1 + \Phi_p \frac{15(1-\nu_0)}{7-5\nu_0} + \rho \left[\frac{16(1-\nu_0)}{15(1-\frac{\nu_0}{2})} + \frac{32(1-\nu_0)}{45} \left(\frac{\delta_c}{1 + \delta_c} \right) \right]. \quad (10)$$

The HF dry elastic moduli K_{HF}^{dry} , K_{HF}^{dry} can be deduced from Eqs. (9) and (10) using $\delta_p \rightarrow \infty$ and $\delta_c \rightarrow \infty$.

2.2. LF moduli calculation: Biot-Gassmann equations

Low frequency (LF) moduli are obtained by taking the HF dry moduli and substituting into Biot-Gassmann equations (Gassmann, 1951). The Biot-Gassmann equations are based on the assumption of uniform pore fluid pressure. Accordingly they are relevant for the saturated isobaric regime and no assumption is made on nature of inclusions. It is a macroscopic approach using only the total porosity value Φ . The dry HF bulk modulus is equal to the dry LF one and the LF saturated bulk modulus K_{LF}^{sat} differs from the dry HF one by:

$$K_{LF}^{sat} = K_{HF}^{dry} + \frac{\beta^2 K_f}{\Phi + (\beta - \Phi) \frac{K_f}{K_0}}, \quad (11)$$

where β is a dimensionless coefficient defined by $\beta = 1 - \frac{K_{HF}^{dry}}{K_0}$.

The LF shear modulus G_{LF}^{sat} is equal to the dry HF shear modulus, and

$$G_{LF}^{dry} = G_{LF}^{sat} = G_{HF}^{dry}. \quad (12)$$

2.3. Frequency dispersion

Based on HF and LF moduli, we are now able to estimate the dispersion resulting from the local flow mechanism. This key parameter is defined as

$$Dispersion = \frac{M_{HF}^{sat} - M_{LF}^{sat}}{M_{LF}^{sat}}, \quad (13)$$

where M is the bulk or shear modulus. In the following parts of this article, we use the short expressions ‘bulk dispersion’ and ‘shear dispersion’ in order to express respectively the dispersion of the bulk and the shear moduli between the two frequency states. We compare only full saturated moduli in order to simplify the interpretation. Note that a frequency dispersion can occur in partially saturated rocks as shown by Le Ravalec and Guéguen (1996a). The measured dispersions are extremely different according to the saturating fluid (Dutta and Odé, 1979; Jones, 1986; Mavko and Mukerli, 1998). In this study we chose to focus on the phenomenon of elastic moduli dispersion with frequency. A lot of studies deal with the notion of attenuation by using the inverse quality factor Q^{-1} . Seismologists use preferentially this parameter. However dispersion and attenuation can be related by using a specific viscoelastic model.

3. Numerical results

For the numerical simulations, we used the elastic parameters of the Icelandic basalt investigated in Adelinet et al. (2010). Those values are presented in Table 1.

3.1. Effect of equant pores on dispersion

We consider in this section the case of a medium containing only equant pores. The porosity varies from 0 to 8%. No dispersion, neither in bulk or in shear moduli, is observed. For shear dispersion, the result is obvious. According to Eq. (4) from the effective medium, and the Eq. (12) from Gassmann model: $G_{HF}^{sat} = G_{BF}^{sat}$, then the dispersion (Eq. (13)) is zero. For the bulk modulus, the result is not so obvious. But it is a consequence of the isotropic shape of the inclusions. This implies that they are isobaric. This can be checked by an exact calculation. Dispersion is equal to zero without any assumption.

Then for a medium containing only equant pores, both hydrostatic stress and anisotropic shear stress fields induce identical fluid pressures in each pore. Therefore, no pore pressure gradients are induced and the dispersion is zero.

3.2. Effect of cracks on dispersion

Let us consider in this section a medium containing only randomly oriented cracks.

The results are summarized in Fig. 4, where the dispersion is plotted versus the crack porosity. The crack porosity is allowed to vary from 0 to 8%. We also assess the validity of the effective medium

Table 1

Input data of the CPEM (based on the elastic properties of an Icelandic basalt). Moduli of the crack and pores-free matrix are given in GPa.

K_0	G_0	K_f
48.8	27.9	2.2

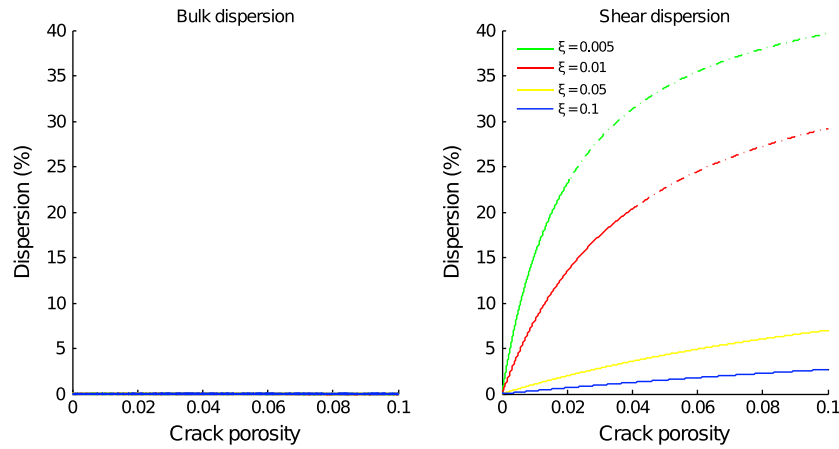


Fig. 4. Numerical results obtained with only cracks added in the EM model. No bulk dispersion is calculated whereas the shear dispersion increases with the crack fraction leading to an asymptotic value. Moreover the smaller aspect ratio, the higher shear frequency dispersion.

theory by testing low aspect ratio value (up to $5 \cdot 10^{-3}$) and high crack porosity (8%), which correspond to a maximum value in crack density ρ of about 4 following Eq. (5). Then we plotted the numerical results with plain curves when $\rho < 1$ and with dashed curves when $\rho > 1$ (limits of the model).

No dispersion in bulk modulus is observed. This can be explained by two factors. First, cracks are randomly distributed and have all the same aspect ratio for each simulation. Second, the bulk sensitivity is linked to an isotropic compression. Then the fluid pressure is the same in all the cracks. As a consequence an isotropic stress field induces no dispersion in a medium composed only by cracks randomly distributed. However a

dispersion in G is observed. Shear dispersion appears to be an increasing function of crack porosity. In this case, an anisotropic shear stress can induce different fluid pressure in cracks according to their orientation. Our results are consistent with other theoretical studies based on different models (O’Connell and Budiansky, 1977; Johnston et al., 1979; Endres and Knight, 1997; Chapman et al., 2002).

The Fig. 5 presents a sketch of the elastic behaviors of round pores and cracks in a hydrostatic or an anisotropic stress field. A frequency dispersion only occurs in G for the cracks medium. This dispersion is strongly dependent on the crack fraction, a point that will be considered in more detail below with the CPEM calculations.

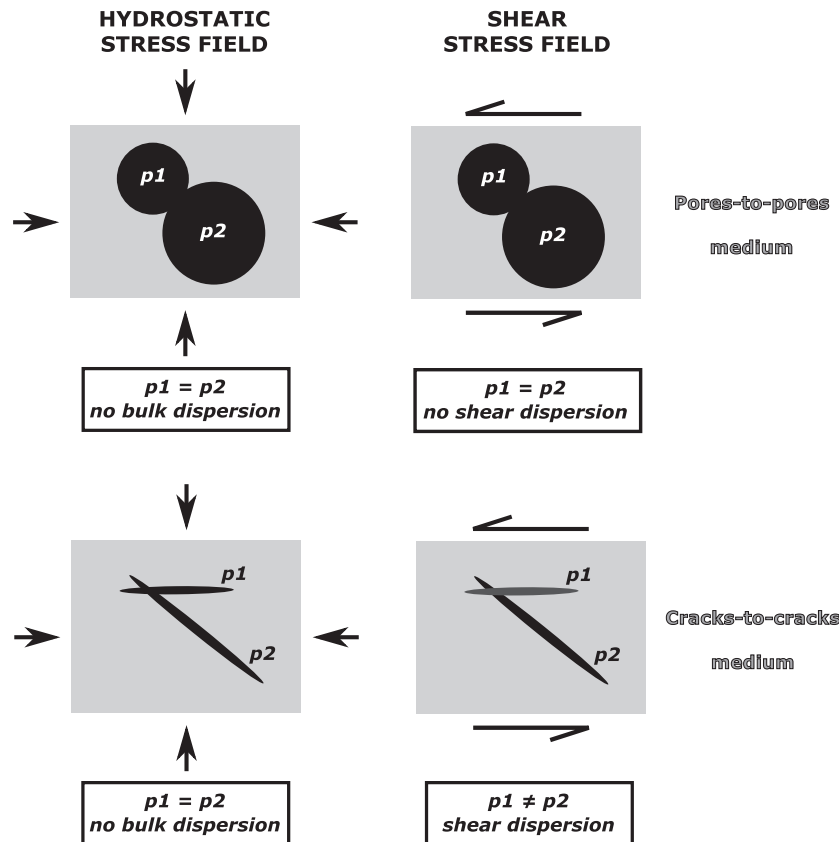


Fig. 5. Sketch of the elastic behavior of round pores and cracks to stress fields (isotropic on the left column and anisotropic on the right column). As cracks are more sensitive to shear stress field than round pores, pore pressure inside cracks is different explaining the frequency dispersion theoretically observed for shear modulus.

3.3. Frequency dispersion for a cracked-porous medium

To investigate the frequency dispersion in a cracked-porous medium, we defined the crack fraction R as $R = \frac{\Phi_{cr}}{\Phi}$. $R=0$ for a medium only composed by equant pores and $R=1$ for a medium only composed by cracks randomly distributed. In the following numerical simulations, the total porosity is fixed to 8%. Fig. 6 presents the computations made for bulk dispersion. We plotted our theoretical predictions for different values of aspect ratio: $5 \cdot 10^{-3}$, $5 \cdot 10^{-2}$ and 10^{-2} . When $R=0$ or 1, the dispersion is zero as demonstrated in the previous sections. However when both equant pores and cracks are present, a bulk dispersion appears and reaches a maximum for a particular intermediate value of the crack fraction. This bulk dispersion is due to a squirt flow from cracks to pores. Indeed the induced fluid pressure in the cracks is greater than the fluid pressure in the equant pores, leading to a HF bulk modulus greater than the LF bulk modulus (calculated from an equilibrated fluid pressure state). Moreover, this bulk dispersion is strongly sensitive to the geometry of the inclusions. At low crack fraction, the amplitude of the dispersion increases rapidly with crack porosity. And the flatter are the cracks (small aspect ratio), the higher is the dispersion. For instance, using cracks with aspect ratio of $5 \cdot 10^{-3}$, the maximum dispersion value is 53%. Note that the maximum dispersion values are always obtained within the validity domain of effective medium theory (plain curves).

Fig. 7 presents the shear dispersion calculated using the CPEM. The boundary conditions (when $R=0$ or 1) are those obtained in the previous sections. When $R \in]0; 1[$, the G dispersion is an increasing function of the crack fraction. The dispersion value is maximum for $R=1$ and reach around 40% for $\xi = 5 \cdot 10^{-2}$. In this case, the maximum value is out the range of validity of the NIA effective medium model. As observed for the bulk dispersion, we note a strong sensitivity to the crack geometry. If cracks have a low aspect ratio, shear dispersion can be very high. On the contrary, if cracks have a high aspect ratio ($\xi \geq 5 \cdot 10^{-3}$), dispersion is very small, less than 5%.

4. Discussion

4.1. Comparison with the study of Endres and Knight (1997)

A key requirement for our model validation is to know if our results are consistent with other theoretical data based on a different approach. We chose to base our comparison on Endres and Knight (1997)'s study which is a generalization of the paper by (Budiansky and O'Connell (1980) using the model of Kuster and Toksoz (1974).

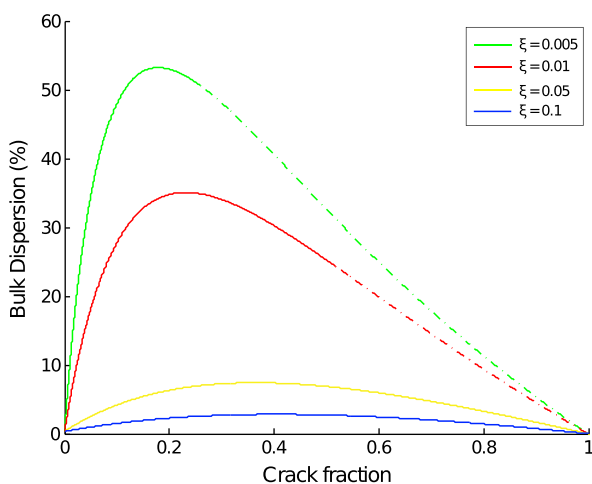


Fig. 6. Numerical results obtained for the CPEM model in bulk modulus. There is no bulk dispersion when $R=0$ or $R=1$ (medium with respectively only pores and only cracks). As seen before, the dispersion increase with smaller aspect ratio values.

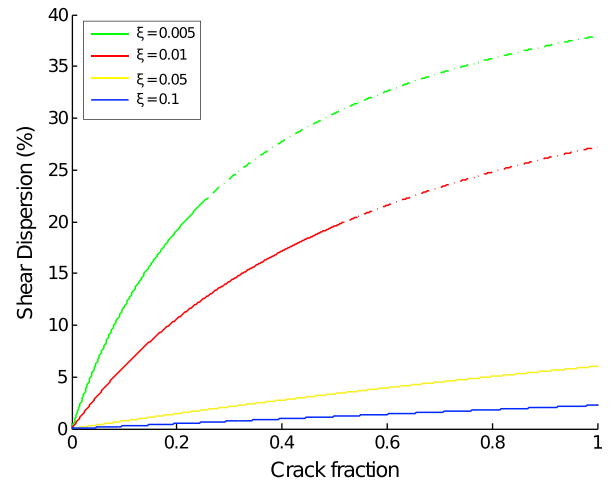


Fig. 7. Numerical results obtained for the CPEM model in shear modulus. The computations are the same as those obtained for a cracks-to-cracks medium: shear dispersion increase with R .

Their formulae are valid for distributions of inclusions with any aspect ratio between 0 and 1. They consider the case where the total porosity is fixed (to 10%) and the geometrical configuration of that porosity is allowed to vary, with aspect ratio ranging from 0.1 to 0.003 (Chapman et al., 2002). The matrix parameters used in Endres and Knight (1997)'s study are summarized in the Table 2. We inferred the crack density values used in their study assuming that cracks are spheroidal (Eq. (5)). For aspect ratio lower than 0.01, the crack density is higher than 1 (Table 3), which is unrealistic.

Fig. 8 presents the comparison between the two models for the bulk dispersion. The trend of bulk dispersion is the same in both models, but the maximum values are different. Our computations are always greater than Endres and Knight (1997)'s ones by about 25%. The reason lies in the LF modulus calculation. We chose to apply directly the Gassmann's equations whereas Endres and Knight (1997) develop their proper relationships which tend towards Gassmann's formulations under some assumption based on microstructure of inclusions. For the shear dispersion calculations, both approaches converge. Due to the equality between LF and HF shear modulus (Eq. (12)), both models are in agreement.

4.2. Experimental data vs. theoretical predictions

In this section, experimental data are compared to the numerical results. For this we use data from an experiment performed on an Icelandic basalt (Adelinet et al., 2010). The rock microstructure is characterized by a bimodal porosity: 1% of cracks and 7% of equant pores. During hydrostatic loading, both saturated HF and LF bulk moduli were measured: HF from velocity measurements and LF from oscillation tests. From experimental data and the previous model, we can estimate crack parameters during loading (*i.e.* crack density and aspect ratio). Two inversion processes were investigated involving each different models: the first one introduced by Fortin and Guéguen (2007) refers to penny-shaped cracks and uses a direct method (called 'simple inversion' on Fig. 9), the second one described in this paper handles spheroidal cracks and uses the minimization of an objective function defined

Table 2

Matrix elastic moduli used in Endres and Knight (1997) (sandstone type). Moduli of the crack and pores-free matrix are given in GPa.

K_0	G_0	Fluid (K_f)
30	17	2.32

Table 3

Crack densities calculated with values used in [Endres and Knight \(1997\)](#). The porosity is fixed to 0.1 with different aspect ratio, ranging from 0.1 to 0.003. Considering spheroidal cracks, crack density is inferred using $\rho = \frac{4}{3}\xi\pi$.

Aspect ratio	0.1	0.03	0.01	0.003
Crack density	0.2	0.8	2.4	8.0

against aspect ratio. This one calculates the least-square difference between the HF measured elastic moduli (K_{me} , G_{me}) and the ones predicted by the CPEM (K_{sim} , G_{sim}):

$$J(\xi) = \frac{1}{2} [c_k(K_{me} - K_{sim})^2 + c_g(G_{me} - G_{sim})^2], \quad (14)$$

where (c_k , c_g) are weighting coefficients taken equal to 1 as first approximation. The aspect ratio value providing the lowest objective function is the optimal solution. We chose to obtain the minimization of $J(\xi)$ by PSO, Particle Swarm Optimization ([Shaw and Srivastava, 2007](#)). [Fig. 9](#) displays the crack densities and crack aspect ratios determined from inversion processes. When the effective pressure is in the range [0–100 MPa], the crack aspect ratios deduced from the two inverted models behave the same way. For $P_{eff} > 100$ MPa, discrepancies appear. The first inverted model does not lead to important variations in the aspect ratio over the [100–150 MPa] range. The ξ values are around 10^{-2} . However, the second inverted model emphasizes a significant aspect ratio increase above $P_{eff} = 90$ MPa, up to a value of 1 (equant pores) at $P_{eff} = 130$ MPa. These results are consistent with the crack closure phenomenon. Indeed a link between crack aspect ratio ξ and closure pressure P_c has been formalized by ([Walsh, 1965](#)) as $P_c \sim E_0\xi$. This means that an effective pressure of 100 MPa would be expected to close a crack of aspect ratio near from 2.10^{-3} . Consequently it can be the preferential closure of such thin cracks that results in the inferred increase of the average crack aspect ratio from $7.5 \cdot 10^{-3}$ at low effective pressure to $1.5 \cdot 10^{-2}$ at higher effective pressures ([Fig. 10](#)). Finally two phases can be discerned during the hydrostatic loading experiment: (1) between 0 and 100 MPa, thin cracks are open, squirt-flow can occur and frequency dispersion is observed; and (2) from 100 to 150 MPa, thin cracks are closing, no fluid pressure gradients are induced and frequency dispersion decreases.

During the experiment, porosity was also deduced from strain gauges measurements. During loading, the reduction of porosity is

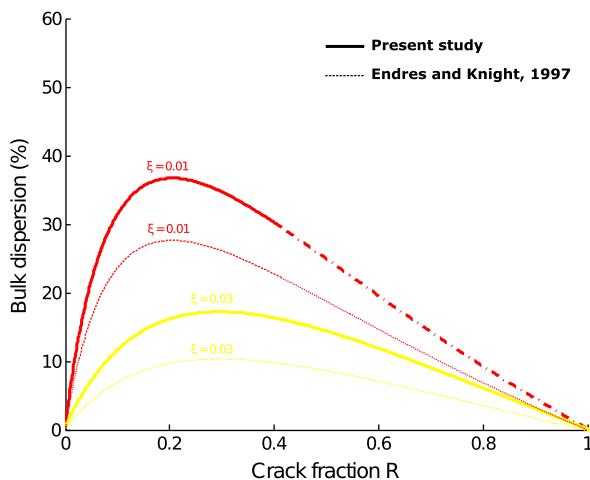


Fig. 8. Comparison in bulk dispersion between theoretical predictions computed using [Endres and Knight \(1997\)](#)'s model (dashed curves) and using CPEM model (plain curves). Crack aspect ratio are denoted above curves.

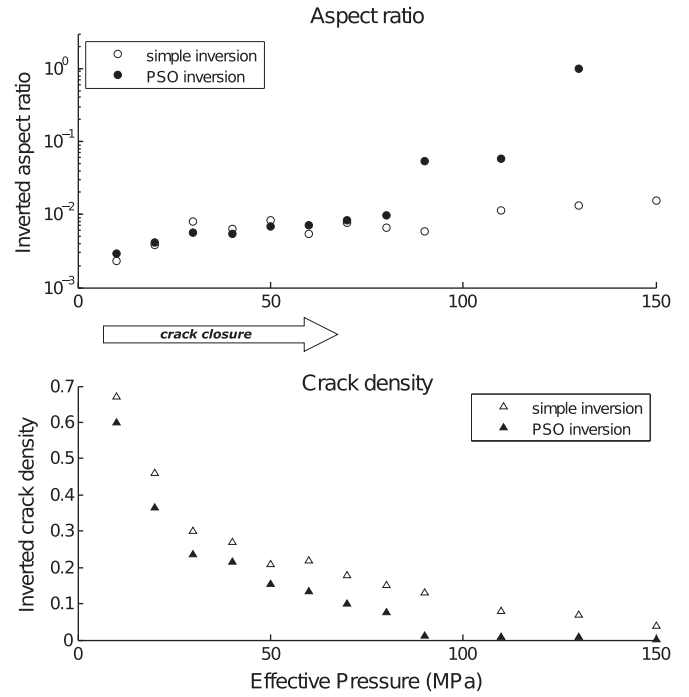


Fig. 9. Inversion of experimental data using two methods. Aspect ratio and crack density are plotted against effective pressure. The empty and plain symbols represents the results obtained respectively by the simple inversion and the Particle Swarm Optimization. Note that PSO is better to discretize the behavior of cracks and equant pores.

about 1%, a value which corresponds to the initial crack porosity. Then assuming that equant porosity do not vary during loading, the total porosity evolution corresponds to a crack porosity evolution, *i.e.* to the crack closure. In the experimental study we have only access to the dispersion of the bulk modulus as we measured the LF bulk modulus by oscillating tests of the confining pressure (no measurements of the LF shear modulus). Then the bulk dispersion can be plotted against crack fraction evolution and also compared directly to theoretical predictions. [Fig. 10](#) presents this comparison. The maximum crack fraction of the investigated rock is 0.125 and corresponds to the initial ratio ($\Phi_{cr} = 1\%$ and $\Phi_p = 7\%$). Then [Fig. 10](#) is a focus on the [0; 0.125] crack fraction range of the [Fig. 6](#).

Note that the general features predicted with the CPEM model are reproduced by the experimental data. Using modeling, the crack aspect ratio can be deduced for the basaltic sample. It is found to increase from $7.5 \cdot 10^{-3}$ (low effective pressure) to $1.5 \cdot 10^{-2}$ (high effective pressure). Then aspect ratio change slightly during loading. These results are consistent with values obtained previously by inversion from HF velocities measurements. From a physical point of view, cracks have two states in the studied rock: open when a low isotropic stress field is applied and closed above a given value of confining pressure (about 130 MPa).

5. Extrapolation to elastic waves velocities and $\frac{V_p}{V_s}$ ratio dispersions

Based on our HF and LF calculations, P and S waves velocities (respectively V_p and V_s) can be deduced using K and G from the well-known following equations:

$$V_p = \sqrt{\frac{K + \frac{4}{3}G}{\mu}}, \quad (15)$$

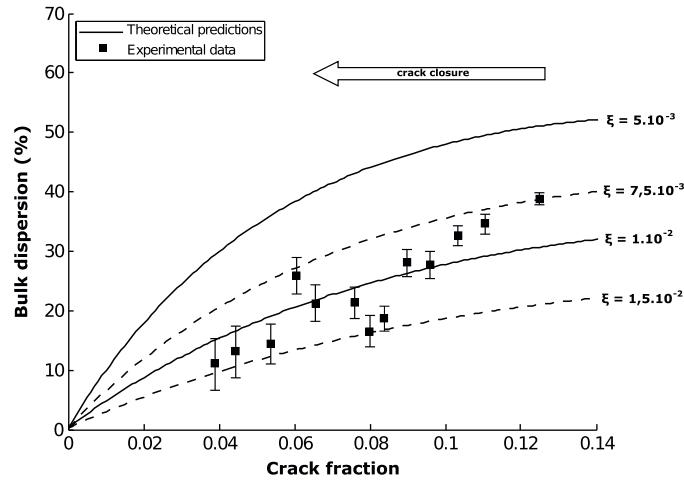


Fig. 10. Comparison between experimental data and theoretical predictions for bulk dispersion in a cracked-porous rock. Aspect ratios are mentioned near from curves. The experimental data are obtained using strain measurements during the loading of a basalt sample (Adelinet et al., 2010). Assumption is made that equant porosity does not change. Then the porosity evolution corresponds to the crack porosity evolution.

$$V_s = \sqrt{\frac{G}{\mu}} \quad (16)$$

where μ is the medium density. We take $\mu = 2700 \text{ kg m}^{-3}$ for our calculations. The velocity dispersion is defined as $\frac{V_{HF}^i - V_{LF}^i}{V_{LF}^i}$. The subscript i refers to either P- and S-waves. In crustal conditions, cracks are always present in the rock microstructure. They represent a small amount of the total porosity, typically around 1 or 2% (Schubnel and Guéguen, 2003). Then we chose to represent velocity dispersion (and V_p/V_s dispersion) on the crack fraction range [0–0.2]. As total porosity is fixed to 8%, it represents a maximum crack porosity of 1.6%, which is near from the maximum values encountered in the natural case. Fig. 11 reports the calculation of the elastic P and S waves dispersion. We observed that V_p and V_s dispersions are increasing function of the crack fraction. V_p dispersion are higher than V_s dispersion due to the additional effect of the dispersion in K and in G . A maximum value of about 18% is achieved for P-wave (using $5 \cdot 10^{-3}$) whereas the maximum dispersion for S-wave and for the same aspect ratio is only 8%.

Our results are consistent with other models developed for isotropic rocks which suggest that a small crack effect (small crack fraction in our case) results in a large dispersion of the seismic wave

velocities (Mavko and Jizba, 1991; Thomsen, 1995; Le Ravalec and Guéguen, 1996b; Sams et al., 1997; Rathore et al., 2006).

The high velocity dispersion predicted by our computations seems also to be in agreement with experimental results. Winkler (1986) indeed observed that several rocks have as much as about 20% dispersion. Furthermore, in our experimental and theoretical studies, the frequency effect is more important for compressional waves than for shear waves as mentioned by other authors (Lucet and Zinszner, 1992).

Based on our model, we examine also the V_p/V_s ratio dispersion. Fig. 12 reports the computations. Note that the dispersion increase for high values of crack fraction, such as reported in Le Ravalec et al. (1996) which used a differential self-consistent model. Moreover, the V_p/V_s dispersion reaches a maximum value of 8.8% for a crack fraction of 0.12 when crack ratio is equal to $5 \cdot 10^{-3}$. With a total porosity fixed to 8%, it corresponds to a crack porosity of 1%. The theoretical predictions explain also why V_p/V_s values can be extremely different from laboratory frequencies measurements to seismic frequencies survey (Takei, 2002).

6. Conclusion

Using effective medium theory and poroelasticity theory, high and low frequency elastic moduli were calculated. Then frequency

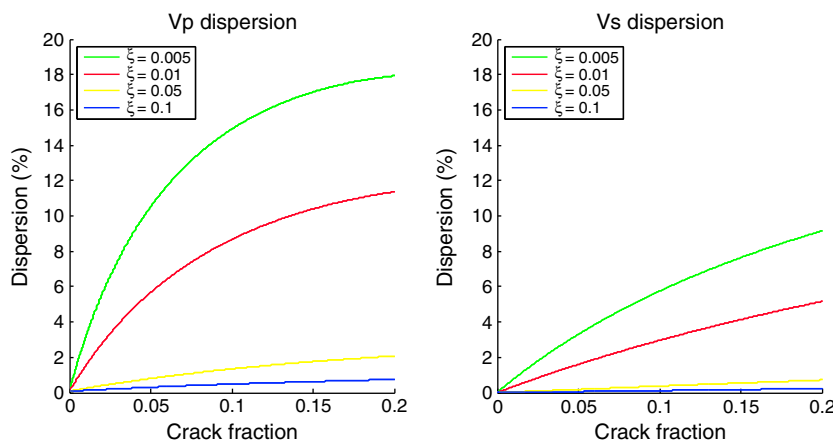


Fig. 11. Numerical extrapolation for seismic waves dispersion. The computation are made on the [0–0.2] crack fraction range which corresponds to the common range encountered in crustal rocks.

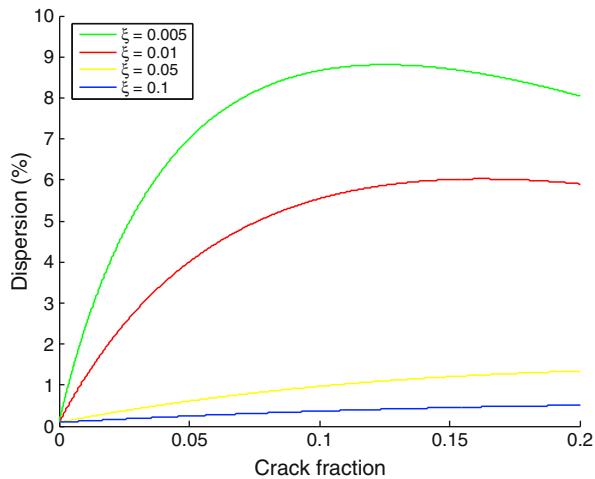


Fig. 12. Numerical extrapolation for $\frac{V_p}{V_s}$ dispersion.

dispersion was derived. As a first conclusion, in the general case where cracks are present in a medium, the frequency dispersion can be very large. Our predicted dispersions are strong and depend on the crack parameters of the rock, *i.e.* the aspect ratio and the crack fraction.

For natural crack fraction (<0.2), our theoretical predictions show that we have to expect discrepancies between data measured at high frequency (in the laboratory or in the wells) and data from the field (seismological survey) at low frequency. The dispersion can reach 20% in the case of P-waves velocities and 10% for the V_p/V_s ratio. This last parameter is very useful to identify fluid processes in depth, such as magma displacement or hydrocarbon flows.

Acknowledgements

The authors thank Mickaële Le Ravalec (IFP Energies nouvelles) for her help in data inversion and PSO algorithm development. They also would like to thank the two reviewers for their constructive comments that helped to improve the paper. This work has been supported by Geoflux - Pays de la Loire and by 3F project SIMULAB of INSU.

References

- Adelinet, M., Fortin, J., Guéguen, Y., Schubnel, A., Geoffroy, L., 2010. Frequency and fluid effects on elastic properties of basalt: experimental investigations. *Geophys. Res. Lett.* 37 (L02303). doi:10.1029/2009GL041660. January.
- Biot, M., 1956. Theory of propagation of elastic waves in a fluid saturated porous solid. 2, higher frequency range. *J. Acoust. Soc. Am.* 28, 168–178.
- Bristow, J., 1960. Microcracks, and the static and dynamic elastic constants of annealed and heavily cold-worked metals. *J. Appl. Phys.* 11, 81–85.
- Budiansky, B., O'Connell, R., 1976. Elastic moduli of a cracked solid. *Int. J. Solids Struct.* 12, 81–97.
- Budiansky, B., O'Connell, R., 1980. Bulk dissipation in heterogeneous media. *Solid Earth Geophys. Geotechnol.* 42, 1–10.
- Chapman, M., Zaitsep, S., Crampin, S., 2002. Derivation of a microstructural poroelastic model. *Geophys. J. Int.* 151, 251–427.
- Dutta, N., Odé, H., 1979. Attenuation and dispersion of compressional waves in fluid-filled porous rocks with partial gas saturation (white model) — part II: results. *Geophysics* 44, 1789–1805.
- Dvorkin, J., Nur, A., 1993. Dynamic poroelasticity: a unified model with the squirt and biot mechanisms. *Geophysics* 58, 524–533.

- Dvorkin, J., Mavko, G., Nur, A., 1995. Squirt flow in fully saturated rocks. *Geophysics* 60 (1), 97–107.
- Endres, A., Knight, R., 1997. Incorporating pore geometry and fluid pressure communication into modeling the elastic behavior of porous rock. *Geophysics* 62, 106–117.
- Eshelby, J., 1957. The determination of the elastic field of an ellipsoidal inclusion, and related problems. *Proc. R. Soc. Lond.* 241, 376–396.
- Fortin, J., Guéguen, Y., 2007. Effects of pore collapse and grain crushing on ultrasonic velocities and $\frac{V_p}{V_s}$. *J. Geophys. Res.* 112 (B0), 8207. doi:10.1029/2005JB004005.
- Gassmann, F., 1951. Über die elasticität poröser medien. *Vierteljahrschr. Naturforsch. Ges. Zurich* 96, 1–23.
- Guéguen, Y., Dienes, J., 1989. Transport properties of rocks from statistics and percolation. *Math. Geol.* 21, 1–13.
- Guéguen, Y., Chelidze, T., Le Ravalec, M., 1997. Microstructures, percolation thresholds, and rock physical properties. *Tectonophysics* 279, 23–35.
- Guéguen, Y., Sarout, J., Fortin, J., Schubnel, A., 2009. Cracks in porous rocks: tiny defects, strong effects. *Lead. Edge* 40–47.
- Henyey, F., Pomphrey, N., 1982. Self-consistent elastic moduli of a cracked solid. *Geophys. Res. Lett.* 9, 903–906.
- Johnston, D., Toksoz, M., Timur, A., 1979. Attenuation of seismic waves in dry and saturated rocks: II. Mechanisms. *Geophysics* 44, 691–711.
- Jones, T., 1986. Pore fluids and frequency-dependent wave propagation in rocks. *Geophysics* 51, 1939–1953.
- Kachanov, M., 1980. Continuum model of medium with cracks. *J. Eng. Mech. Div.* 106, 1039–1051.
- Kachanov, M., 1993. Elastic solids with many cracks and related problems. Vol. *Advances in Applied Mechanics*. Academic Press, Boston, MA, pp. 259–445. Ch. 30.
- Kachanov, M., Tsukrov, I., Shafiro, B., 1994. Effective moduli of solids with cavities of various shapes. *Appl. Mech. Rev.* 47, 151–174.
- Kuster, G., Toksoz, M., 1974. Velocity and attenuation of seismic waves in two phases media: part I. Theoretical formulations. *Geophysics* 39, 587–606.
- Le Ravalec, M., Guéguen, Y., 1996a. Elastic wave velocities in partially saturated rocks: saturation hysteresis. *J. Geophys. Res.* 101, 837–844.
- Le Ravalec, M., Guéguen, Y., 1996b. High- and low-frequency elastic moduli for a saturated porous/cracked rock — differential self-consistent and poroelastic theories. *Geophysics* 61, 1080–1094.
- Le Ravalec, M., Guéguen, Y., Chelidze, T., 1996. Magnitude of velocity anomalies prior to earthquakes. *J. Geophys. Res.* 101 (B5), 11217–11223.
- Lucet, N., Zinszner, B., 1992. Effects of heterogeneities and anisotropy on sonic and ultrasonic attenuation in rocks. *Geophysics* 57 (8), 1018–1026.
- Mavko, G., Jizba, D., 1991. Estimating grain-scale fluid effects on velocity dispersion in rocks. *Geophysics* 56, 1940–1949.
- Mavko, G., Mukerli, T., 1998. Bounds of low-frequency seismic velocities in partially saturated rocks. *Geophysics* 63 (3), 918–924.
- Mavko, G., Nur, A., 1975. Melt squirt in asthenosphere. *J. Geophys. Res.* 80, 1444–1448.
- Murphy, W., 1985. Sonic and ultrasonic velocities: theory versus experiment. *Geophys. Res. Lett.* 12 (2), 85–88.
- Norris, A., 1985. A differential scheme for the effective moduli of composites. *Mech. Mater.* 4, 1–16.
- O'Connell, R., Budiansky, B., 1977. Viscoelastic properties of fluid-saturated cracked solids. *J. Geophys. Res.* 82, 5719–5735.
- Rathore, J., Fjaer, E., Holt, R., Renlie, L., 2006. P- and s-wave anisotropy of a synthetic sandstone with controlled crack geometry. *Geophys. Prospect.* 43 (6), 711–728.
- Sams, M., Neep, J., Worthington, M., King, M., 1997. The measurement of velocity dispersion and frequency-dependent intrinsic attenuation in sedimentary rocks. *Geophysics* 62 (5), 1456.
- Schubnel, A., Guéguen, Y., 2003. Dispersion and anisotropy of elastic waves in cracked rocks. *J. Geophys. Res.* 108 (B2).
- Shafiro, B., Kachanov, M., 1997. Materials with fluid-filled pores of various shapes: effective elastic properties and fluid pressure polarisation. *Int. J. Solids Struct.* 34, 3517–3540.
- Shaw, R., Srivastava, S., 2007. Particle swarm optimization: a new tool to invert geophysical data. *Geophysics* 72 (2).
- Takei, Y., 2002. Effect of pore geometry on v_p/v_s : from equilibrium geometry to crack. *J. Geophys. Res.* 107 (B2).
- Thomsen, L., 1995. Elastic anisotropy due to aligned cracks in porous rock. *Geophys. Prospect.* 43, 805–829.
- Walsh, 1965. The effect of cracks on the compressibility of rock. *J. Geophys. Res.* 70, 381–389.
- Winkler, K., 1986. Estimates of velocity dispersion between seismic and ultrasonic frequencies. *Geophysics* 51, 183–189.
- Zimmerman, R., Somerton, W., King, M., 1986. Compressibility of porous rocks. *J. Geophys. Res.* 91 (12), 12,765–12,777.